HHS Public Access

Author manuscript

Nat Neurosci. Author manuscript; available in PMC 2017 October 03.

Published in final edited form as:

Nat Neurosci. 2017 May ; 20(5): 708–716. doi:10.1038/nn.4540.

GLP-1 acts on habenular avoidance circuits to control nicotine intake

Luis M. Tuesta[1,2], **Zuxin Chen**[5], **Alexander Duncan**[5], **Christie D. Fowler**[1], **Masago Ishikawa**[5], **Brian R. Lee**[1], **Xin-An Liu**[5], **Qun Lu**[1], **Michael Cameron**[1], **Matthew R. Hayes**[4], **Theodore M. Kamenecka**[1], **Matthew Pletcher**[1,3], and **Paul J. Kenny**[1,5,*]

[1]Department of Molecular Therapeutics, The Scripps Research Institute, 130 Scripps Way, Jupiter, FL 33458, USA

[2]The Kellogg School of Science and Technology, The Scripps Research Institute, 130 Scripps Way, Jupiter, FL 33458, USA

[3]Autism Speaks, Boston, MA 02109

[4]Department of Psychiatry, Perelman School of Medicine, University of Pennsylvania, Philadelphia, PA 19104

Abstract

Tobacco smokers titrate their nicotine intake to avoid its noxious effects, sensitivity to which may influence vulnerability to tobacco dependence, yet mechanisms of nicotine avoidance are poorly understood. Here, we show that nicotine activates glucagon-like peptide-1 (GLP-1) neurons in the nucleus tractus solitarius (NTS). The antidiabetic drugs sitagliptin and exenatide, which inhibit GLP-1 breakdown and stimulate GLP-1 receptors (GLP-1Rs), respectively, decrease nicotine intake in mice. Chemogenetic activation of GLP-1 neurons in NTS similarly decreases nicotine intake. Conversely, *Glp1r* knockout mice consume greater quantities of nicotine than wild-type mice. Using optogenetic stimulation, we show that GLP-1 excites medial habenular (MHb) projections to interpeduncular nucleus (IPN). Activation of GLP-1Rs in the MHb-IPN circuit abolishes nicotine reward and decreases nicotine intake, whereas their knockdown or pharmacological blockade increases intake. GLP-1 neurons may therefore serve as “satiety sensors” for nicotine that stimulate habenular systems to promote nicotine avoidance before its aversive effects are encountered.

Tobacco smoking is the primary cause of preventable death and disease in developed nations, costing approximately $100 billion in annual health care expenses in the United

*Correspondence should be addressed to: PJK (paul.kenny@mssm.edu).

[5]Present address: Department of Neuroscience, Icahn School of Medicine at Mount Sinai, One Gustave L. Levy Place, New York, NY 10029.

Contributions

L.M.T., A.D., Z.C., C.D.F., B.R.L., X.L., Q.L. and M.I. conducted all experiments. T.M.K., M.C., M.P. and M.R.H. provided essential reagents. L.M.T. and P.J.K. designed the experiments, analyzed the data and wrote the manuscript.

Competing financial interests

The authors declare no competing interests.

States alone. Nicotine is the major rewarding component in tobacco smoke that drives the development of tobacco addiction [1]. Rewarding effects of nicotine are regulated by neuronal nicotinic acetylcholine receptors (nAChRs) containing β2 subunits (denoted β2* nAChRs) located in the ventral tegmental area (VTA) [2]. In addition to its rewarding effects nicotine also has aversive effects that promote avoidance [3, 4]. Smokers are far more efficient at titrating their intake downward when consuming tobacco high in nicotine content than at adjusting their intake upward to compensate for reduced nicotine content [3, 4]. Stronger aversive reaction to nicotine after initial tobacco use decreases the likelihood of progressing to habitual use [3, 4]. Conversely, genetic variation that decreases sensitivity to noxious effects of nicotine increases vulnerability to tobacco dependence [4]. These findings suggest that avoiding noxious effects of nicotine plays a key role in determining patterns and amounts of tobacco consumption and may regulate vulnerability to addiction. Nevertheless, in contrast to the well-defined mechanisms of nicotine reward, very little is currently known about mechanisms of nicotine avoidance.

The NTS is a hindbrain region that receives vagal innervation delivering sensory input from the oral cavity, lungs, gut and heart, all sites involved in introceptive actions of nicotine contained in tobacco smoke. The NTS is known to regulate feeding behaviors, most notably the sensation of fullness (satiety), that promote meal termination [5]. NTS neurons also regulate avoidance behaviors, including avoiding locations associated with punishing footshocks or food adulterated with noxious lithium chloride. nAChRs are densely expressed in NTS, particularly those containing α5, α3 and/or β4 subunits that were recently implicated in regulating noxious responses of nicotine [4, 6]. Here, we investigated the role of the NTS in regulating nicotine avoidance.

RESULTS

Nicotine activates GLP-1 neurons in the NTS

We first assessed the responsiveness of NTS neurons to nicotine using Fos immunoreactivity as a marker of neuronal activation. We found that nicotine (0.25 and 1.5 mg kg^{-1}) increased numbers of Fos-immunopositive (Fos+) cells in caudal NTS (cNTS; Fig. 1b) and rostral NTS (rNTS; Supplementary Fig. 1). A prominent population of neurons in cNTS are those that synthesize glucagon-like peptide-1 (GLP-1) [7] (Fig. 1a). We detected a significant number of GLP-1+ neurons that were Fos+ in response to nicotine (Fig. 1b, c). Using *Chrna5*-EGFP transgenic mice, in which the promoter of the α5 nAChR subunit gene drives GFP expression, we detected GFP+ neurons that were also immunoreactive for GLP-1 (Supplementary Fig. 2). This suggests that α5* nAChRs, and perhaps other nAChR subtypes, are expressed by GLP-1 neurons and are activated by nicotine. Another prominent population of NTS neurons are catecholaminergic and express tyrosine hydroxylase (TH) (Fig. 1a). Nicotine-induced Fos immunoreactivity was largely absent from TH-positive (TH +) neurons in cNTS (Fig. 1b), with only ~5% of detected TH+ neurons also Fos+ (Fig. 1c). Similarly, Fos was sparsely detected in TH+ neurons in rNTS (Supplementary Fig. 1). However, nicotine increased the numbers of TH+ neurons that were Fos+ in the ventrolateral medulla (VLM) (Fig. 1b). These findings suggest that nicotine activates NTS neurons but acts preferentially on GLP-1 neurons rather than catecholaminergic neurons (Fig. 1c). It is

noteworthy that a sizable fraction of Fos+ NTS neurons were neither GLP-1+ nor TH+ (Fig. 1c), and we detected *Chrna5*-GFP+ neurons that were not immunoreactive for GLP-1. Together, these findings demonstrate that nicotine activates GLP-1 neurons and at least one other population of non-TH+ neurons in the NTS.

GLP-1 regulates nicotine intake

Circulating GLP-1, which is rapidly degraded by the enzyme dipeptidyl peptidase-4 (DPP4), enhances insulin secretion and sensitivity [8] (Fig. 2a). Based on this action, drugs that block DPP4, such as sitagliptin (Januvia), or that mimic the actions of GLP-1 by stimulating GLP-1 receptors (GLP-1Rs), such as exenatide (exendin-4; Byetta), are used clinically for the treatment of type 2 diabetes (T2D) (Fig. 2a). Exendin-4 (Ex4) (≤10 μg kg^{-1}) is known to attenuate reduces the rewarding effects of nicotine, cocaine, amphetamine and alcohol in rodents, measured using place conditioning procedures [9–11]. Therefore, we investigated the role for GLP-1 transmission in regulating the motivational properties of nicotine.

In mice lever-pressing for nicotine under a fixed ratio 5 time-out 20 sec (FR5TO20) schedule of reinforcement (Fig. 2b), we found that Ex-4 (10 μg kg^{-1}) decreased nicotine intake (Fig. 2c) but did not alter responding for food rewards (20 mg chow pellets) (Supplementary Fig. 3). Similarly, sitagliptin (10 mg kg^{-1}) also decreased nicotine self-administration in mice (Fig. 2d). These findings are consistent with an inhibitory action of GLP-1 transmission on nicotine intake. We also found that *Glp1r* KO mice consumed more nicotine than their wild-type littermates across a range of nicotine doses, resulting in an upward shift in the dose-response curve (Fig 2e). By contrast, responding for food rewards was similar between *Glp1r* KO and wild-type mice when tested under the same FR5TO20 reinforcement schedule (Fig. 2f). Interestingly, nicotine (0.25 mg kg^{-1} SC) decreased responding for food similarly in wild-type and *Glp1r* KO mice (Supplementary Fig. 4), suggesting that GLP-1 is likely not involved in the anorectic effects of nicotine. Together, these findings support a role for GLP-1 transmission in regulating the motivational properties of nicotine.

Chemogenetic stimulation of GLP-1 neurons decreases nicotine intake

In addition to brain, GLP-1 receptors are expressed in intestine, liver, lung, pancreas and kidney [12], making it unclear if GLP-1 influences nicotine intake through actions inside or outside the brain. To address this issue we used designer receptors exclusively activated by designer drugs (DREADDs) to place GLP-1 neurons under experimenter control. To selectively target GLP-1 neurons with DREADDs, we used a line of Phox2b-Cre mice in which the Cre transgene in NTS is reported to be expressed selectively in GLP-1+ neurons [13]. To confirm this specificity of expression we bred the Phox2b-Cre mice with a line of ROSA-tdTomato mice in which the fluorescent protein tdTomato (tdTom) is expressed in a Cre-dependent manner. We found that the majority of tdTom+ neurons in these mice were immunopositive for GLP-1 and immunonegative for TH (Supplementary Fig. 5). However, we detected occasional TH+ neurons that were tdTom+ (Supplementary Fig. 5), suggesting that populations of TH+ (and perhaps other non-GLP-1) cells may express Cre in the NTS of these mice.

To compare the effects of selectively activating of GLP-1 neurons with more generalized activation of the NTS we injected AAV-DIO-hM3Dq-mCitrine (Cre-dependent) or AAV-hM3Dq-mCitrine (non-Cre-dependent) excitatory DREADDs into the cNTS of Phox2b-Cre mice (Fig. 3a). We detected prominent fluorescence in GLP-1 neurons of the in the DIO-hM3Dq-expressing Phox2b-Cre mice (Fig. 3b). By contrast, we detected widespread transduction of NTS neurons in the non-DIO-hM3Dq-expressing Phox2b-Cre mice (Fig. 3c).

Moreover, CNO (1 mg kg^{-1}) markedly decreased nicotine self-administration (0.1 mg kg^{-1} per infusion) in DIO-hM3Dq-expressing Phox2b-Cre mice relative to saline injection (Fig. 3d), whereas only CNO tended to decrease nicotine intake in the DIO-hM3Dq-expressing Phox2b-Cre mice compared with saline injection (p=0.066; Fig. 3e). As expected, CNO had no effects on nicotine intake relative to saline injection in Phox2b-Cre mice that received intra-NTS injections of AAV-EGFP (Fig. 3f). Also, CNO did not alter responding for food rewards in the DIO-hM3Dq- or EGFP-expressing Phox2b-Cre mice (Supplementary Fig. 6). By contrast, CNO decreased food responding in non-DIO-hM3Dq-expressing Phox2b-Cre mice (Supplementary Fig. 6). As small numbers of TH+ neurons in NTS of Phox2b-Cre mice expressed Cre (Supplementary Fig. 5), and Phox2b is reported to be expressed in non-GLP-1+ neurons in NTS and other hindbrain sites [14, 15], it is possible that CNO may have decreased nicotine intake in the DIO-hM3Dq-expressing Phox2b-Cre mice in part by stimulating non-GLP-1 neurons. Therefore, to further confirm a role for GLP-1 neurons in regulating nicotine intake we used mice in which Cre expression is controlled by the preproglucagon (*Gcg*) gene promoter (Gcg-Cre mice), the gene from which GLP-1 is derived. We injected AAV-DIO-hM3Dq-mCherry into cNTS of Gcg-Cre mice and trained them to respond for nicotine infusions as described above (Fig. 3g). As expected, mCherry fluorescence was detected only in GLP-1 neurons in NTS of these mice (Fig. 3g), and CNO significantly reduced their nicotine intake compared with saline injection (Fig. 3h). Together, these findings are consistent with a central site of action for GLP-1 in regulating the motivational properties of nicotine.

GLP-1 stimulates habenular inputs to the interpeduncular nucleus

Next, we investigated the site of action for GLP-1 in brain in controlling nicotine intake. Central GLP-1 receptors demonstrate a relatively restricted expression pattern, with some of the highest densities of binding sites detected in the interpeduncular nucleus (IPN) [7]. Recently, our laboratory established that nicotine-induced stimulation of excitatory inputs from the medial habenula (MHb) to IPN, and consequent activation of IPN neurons, promotes nicotine avoidance [16]. We therefore tested the possibility that GLP-1 may stimulate IPN activity to decrease nicotine intake. We detected GFP+ fibers in the IPN of mice after injection of AAV-GFP into the NTS (Fig. 4a,b), consistent with NTS projections to IPN. We also detected GLP-1-immunoreactive fibers in IPN of mice (Fig. 4c), suggesting that at least a portion of this NTS input comes from GLP-1 neurons. CNO increased Fos immunoreactivity in IPN neurons of Phox2b-Cre mice that received cNTS injection of AAV-DIO-hM3Dq (Supplementary Fig. 7). This suggests that NTS inputs stimulate local neuronal activity in IPN. To more directly investigate this possibility, we injected Cre-inducible channelerhodopsin-2 (DIO-ChR2-GFP) into the NTS of Gcg-Cre mice and tested the effects

of optically stimulating ChR2+ terminals in IPN (Fig. 4d). As expected, GFP from this virus was detected exclusively in GLP-1 neurons in NTS (Fig. 4e) and we detected GFP+ fibers in the IPN of these mice (Fig. 4f). We found that high (20 Hz) (Fig. 4j,k,l) but not low (1 Hz) (Fig. 4g,h,i) intensity opto-stimulation of GFP+ terminals markedly increased the frequency but not the amplitude of excitatory post-synaptic currents (EPSCs) in IPN neurons. As high frequency opto-stimulation (≥ 20 Hz) is usually required to trigger neuropeptide release from terminals these data suggest that GLP-1 released from NTS terminals in IPN increase excitatory currents in IPN neurons.

The data described above suggest that GLP-1 likely acts through a presynaptic mechanism to increase glutamatergic transmission onto IPN neurons. In keeping with a presynaptic site of action, bath application of Ex-4 (100 nM) increased the frequency but not the amplitude of miniature EPSCs (mEPSCs) in IPN neurons (Fig. 5a–e). We next sought to identify the source of excitatory input onto IPN neurons that is stimulated by GLP-1. As high (20 Hz) but not low (1 Hz) frequency opto-stimulation increased EPSCs in IPN, and 1–2 Hz stimulation is usually sufficient to increase glutamate release from excitatory terminals, it is unlikely that GLP-1 terminals are a major source of glutamatergic drive onto IPN neurons. The IPN receives massive cholinergic innervation from MHb via the fasciculus retroflexus [17]. MHb cholinergic neurons co-release glutamate and provide the major source of glutamatergic input to IPN [17]. Therefore, we hypothesized that GLP-1 stimulates habenular terminals to enhance excitatory drive onto IPN neurons. To investigate this possibility we used ChAT-ChR2-YFP mice in which ChR2 and yellow fluorescent protein (YFP) are expressed in cholinergic neurons under the control of the promoter for the choline acetyltransferase (*Chat*) gene. Excitatory currents evoked by optical stimulation of the IPN in ChAT-ChR2-YFP are derived almost exclusively from MHb terminals [17]. We observed dense ChR2 and YFP expression in MHb neurons and on MHb terminals in IPN, but not postsynaptically on local IPN neurons (which are GABAergic) (Fig. 5f), in the ChAT-ChR2-YFP mice. As expected, optical stimulation of IPN slices from these mice evoked a robust EPSC in IPN neurons (Fig. 5g). This effect was markedly enhanced by bath application of Ex-4 (100 nM) (Fig. 5h). Finally, we found that nicotine-induced increases in IPN activity in mice, measured using Fos immunoreactivity, were greatly diminished in *Glp1r* KO mice compared with wild-type controls (Fig. 5i,j). Together, these findings suggest that GLP-1 released from NTS terminals enhances IPN neuron activity by stimulating habenular terminals and that GLP-1 plays a permissive role in the stimulatory effects of nicotine on MHb-IPN circuit activity.

GLP-1 signaling in the MHb-IPN circuit regulates nicotine intake

A parsimonious explanation for how GLP-1 stimulates excitatory habenular inputs to IPN is by activating GLP-1Rs expressed on the terminals of these neurons. Using BAC-TRAP, habenular cholinergic neurons were shown to transcribe modest levels of *Glp1r* mRNA [18]. To directly investigate the functional significance of GLP-1Rs on habenular terminals we tested the effects of knocking down *Glp1r* transcripts in MHb on nicotine intake. We injected AAV-sh-*Glp1r*-GFP or a control AAV-GFP vector into MHb of rats and detected robust GFP expression in MHb and GFP+ fibers in IPN (reflecting terminals of MHb neurons) (Fig. 6a), confirming accurate targeting of virus injections to MHb. We also

detected robust knockdown of *Glp1r* transcripts in MHb of AAV-sh-*Glp1r*-GFP rats compared with AAV-GFP rats (Supplementary Fig. 8). Responding for food reinforcers was similar between rats that received intra-MHb injections of AAV-sh-*Glp1r*-GFP or AAV-GFP (Supplementary Fig. 9). However, nicotine intake was increased in the AAV-sh-*Glp1r*-GFP rats compared with AAV-GFP rats (Fig. 6b), an effect apparent at higher doses of the drug (0.09 and 0.12 mg kg^{-1} per infusion; FR5TO20). These data are consistent with a role for GLP-1 receptors expressed on habenular terminals in regulating the actions of GLP-1 in IPN to control nicotine intake. We also found that infusion of Ex-4 (0.1 μg per 0.5 μl) into IPN (Fig 6c,d), but not 2 mm above the IPN (Fig 6e), dramatically decreased nicotine intake in rats (0.03 mg kg^{-1} per infusion; FR5TO20). Ex-4 acting in the IPN did not alter responding for food rewards (Supplementary Fig. 10). GLP-1 receptor activation is known to stimulate production of the intracellular second messengers cAMP and cGMP [19]. Intra-IPN infusions of 8-Br-cGMP (0.75, 3.0 μg/0.5 μl), a non-hydrolyzable and cell-permeable analog of cGMP, had no effects on nicotine intake in rats (Supplementary Fig. 11). By contrast, co-infusing a behaviorally inactive dose of the cAMP inhibitor cAMPS-Rp (1 μg per 0.5 μl) into IPN completely abolished the inhibitory effects of Ex-4 (0.1 μg per 0.5 μl) on nicotine intake (Fig. 6d). Conversely, infusion of the GLP-1 receptor antagonist exendin-(9–39)-amide (Ex-9; 20 μg per 0.5 μl) into the IPN increased nicotine intake in rats compared with vehicle injection (Fig. 6f), but did not alter food responding (Supplementary Fig. 10). Interestingly, the stimulatory effect of Ex-9 on nicotine intake was not apparent until 24 h after IPN infusion (Fig. 6f). The reason for this delayed onset of action is unclear, but the findings are consistent with an inhibitory action of GLP-1 in IPN on nicotine intake. Together, these data demonstrate that GLP-1 transmission in IPN, and activation of downstream cAMP-regulated signaling cascades, decreases the motivational properties of nicotine.

GLP-1 signaling in the MHb-IPN circuit regulates nicotine reward

Rats and mice regulate their pattern of nicotine self-administration to achieve maximal rewarding effects while avoiding aversive effects of nicotine [1], similar to the careful titration of tobacco intake seen in human smokers. Activation of the MHb-IPN circuit by nicotine [20] contributes to its aversive effects that promote avoidance [21]. Therefore, next investigated the role for GLP-1 transmission in the IPN in regulating the reward-related actions of nicotine, as measured using the intracranial self-stimulation (ICSS) procedure. In this procedure rats respond for rewarding electrical self-stimulation via an intracranial electrode. The minimal stimulation intensity that supports self-stimulation behavior is termed the reward threshold [22–24]. Rewarding doses of nicotine lower ICSS thresholds [1] whereas higher aversive doses of nicotine elevate ICSS thresholds in rats [25]. ICSS thresholds were assessed twice daily in rats that had access to self-administered nicotine infusions (0.03 mg kg^{-1} per infusion) during 1 h sessions, with thresholds assessed immediately before the self-administration session began and again immediately afterwards (Fig. 7a,b). As expected, rats receiving intra-IPN infusion of vehicle before the pre-nicotine ICSS session titrated their nicotine intake to a level that achieved statistically significant lowering of post-nicotine ICSS thresholds compared with pre-nicotine thresholds (Fig. 7c). This lowering of ICSS thresholds reflects the stimulatory effect of nicotine on brain reward systems. When Ex-4 was infused into IPN prior to start of the pre-nicotine ICSS session (Fig. 7a) we found that ICSS thresholds were unaltered by Ex-4 (Fig. 7c). However, nicotine intake during the

subsequent nicotine self-administration was markedly reduced by the Ex-4 infusion (Fig. 7d), replicating the data shown in Fig. 6. Moreover, this Ex-4 infusion completely abolished the lowering of post-nicotine ICSS thresholds typically observed after a nicotine self-administration session (Fig. 7c). Together, these data suggest that GLP-1 transmission in the MHb-IPN circuit decreases nicotine intake not because it is intrinsically aversive or induces a state of malaise similar to that induced by higher doses of nicotine. Instead, GLP-1 likely decreases nicotine intake by reducing the amount that can be consumed before its threshold-elevating (aversive) actions are encountered. In other words, GLP-1 signaling in the MHb-IPN circuit promotes nicotine avoidance.

Discussion

Smokers consume tobacco to obtain nicotine and experience its rewarding effects. The stimulatory effect of nicotine on midbrain dopamine neurons is thought to play a key role in this process. However, a defining feature of the tobacco habit is the careful titration of intake demonstrated by smokers to avoid noxious effects of nicotine. In fact, noxious responses to tobacco after initial exposure is inversely correlated with the propensity to develop habitual use [26]. When smokers inhale more deeply or rapidly than usual, and obtain nicotine beyond their preferred levels, they experience an aversive behavioral state that results in persistent suppression of intake even in smokers with established habits and a long history of nicotine consumption [27]. This suggests that intake is carefully titrated such that the rewarding effects of nicotine can be experienced but its noxious effects avoided. Currently, very little is known about the brain systems that control intake in order to avoid the aversive effects of nicotine. An understanding of these systems is crucial, as adaptations in these systems in response to nicotine intake may facilitate the development of the smoking habit. Moreover, manipulating the activity of such avoidance systems could serve as a strategy to develop novel therapeutics that can facilitate smoking cessation. Here, we show that nicotine stimulates GLP-1 neurons in NTS and that GLP-1 transmission enhances the activity of excitatory habenular inputs to IPN. GLP-1 signaling in IPN, while not intrinsically aversive, completely blocks the rewarding effects of nicotine and promotes nicotine avoidance. These findings suggest that GLP-1 neurons regulate nicotine intake in a manner analogous to their role in meal patterning, serving as “satiety sensors” that facilitate the termination of consummatory behavior before the aversive effects of overconsumption are encountered.

The IPN, located ventromedially to the VTA and containing some of the highest densities of GLP-1 receptor binding sites in the brain [7, 28], was recently shown to play an important role in nicotine avoidance [16]. Indeed, chemical inactivation of the IPN or reduced nAChR signaling throughout the MHb-IPN circuit decreases sensitivity to the aversive effects of nicotine and increases consumption of the drug [16]. Based on these observations we hypothesized that the MHb-IPN circuit serves as an important substrate for the inhibitory actions of GLP-1 on nicotine intake. Consistent with this possibility, optical stimulation of the terminals of GLP-1 neurons in IPN, and the GLP-1R agonist Ex-4, increased EPSCs in IPN neurons through a presynaptic mechanism. Further, Ex-4 increased EPSCs in IPN neurons evoked by optical stimulation of excitatory habenular inputs. Knockdown of *Glp1r* transcripts in MHb neurons or infusion of the GLP-1R antagonist Ex-9 into IPN increased nicotine intake, whereas infusion of Ex-4 into the IPN decreased intake. These findings

suggest that GLP-1 controls nicotine intake, at least in part, by regulating excitatory transmission in IPN derived from habenular inputs.

We found that Ex-4 infused into IPN decreased nicotine intake and abolished the ICSS threshold-lowering (rewarding) effects of nicotine. However, Ex-4 infused into the IPN was not intrinsically aversive, as measured by elevations of ICSS thresholds. These are important observations for two reasons: First, they suggest that engaging MHb-IPN circuit activity can override the rewarding properties of nicotine, but precisely how this occurs is unclear. The IPN provides inhibitory GABAergic projections to the VTA [29], a brain site known to play a critical role in regulating the rewarding properties of nicotine [2]. Therefore, IPN-derived GABAergic transmission onto VTA dopamine neurons could contribute to the inhibitory effects of MHb-IPN circuit activity on nicotine reward. Moreover, it is an interesting possibility that GLP-1 may also act in the VTA to decrease the rewarding effects of nicotine and other drugs of abuse, and attenuate their effects on mesoaccumbens dopamine transmission, by stimulating inhibitory GABAergic transmission derived from IPN inputs. Second, the stimulatory effects of nicotine on glutamatergic transmission in IPN is hypothesized to contribute to aversive (ICSS threshold-elevating) effects of the drug [30, 31]. However, we report here that GLP-1 enhances glutamatergic drive onto IPN neurons similar to the actions of nicotine (Fig. 4 and ref [20]) and yet is not intrinsically aversive. This suggests that nicotine avoidance and nicotine aversion may be dissociable phenomena explained by different underlying mechanisms in the MHb-IPN circuit, with nicotine avoidance but not aversion related to enhanced glutamatergic transmission from habenular terminals in IPN. In addition to glutamate, nicotine also stimulates acetylcholine release from habenular terminals in IPN [17]. Different firing patterns of habenular neurons are required to stimulate glutamate versus acetylcholine release [17], with brief optogenetic stimulation sufficient to elicit glutamate-mediated excitatory currents but more persistent (tetanic) optogenetic stimulation required to trigger acetylcholine-mediated currents [17]. Cholinergic transmission in striatum and cortex is known to regulate states of aversion [32]. Therefore, it is an intriguing possibility that glutamate released in response to nicotine or GLP-1 may be sufficient to promote avoidance behaviors, whereas acetylcholine released in response to nicotine but not GLP-1 induces an aversive behavioral state. The fact that GLP-1 transmission in the IPN can promote nicotine avoidance without having noxious effects is promising from a translational perspective, as novel therapeutics that can promote nicotine avoidance without inducing a negative behavioral state may have utility in promoting smoking cessation. Considering that enhancers of GLP-1 transmission, such as DPP4 inhibitors (Januvia) or GLP-1 mimetics (Byetta), are used for the treatment of T2D, it will be important to determine whether the motivational properties of tobacco are altered in T2D patients treated with these drugs.

GLP-1 neurons in NTS signal satiety states and GLP-1 receptor agonists decrease food intake [33]. Hence, it may have been expected that chemogenetic stimulation of GLP-1 neurons would have decreased responding for food and that *Glp1r* KO mice would have consumed more food than their wild-type counterparts. However, we observed no effects of manipulating GLP-1 receptor-mediated transmission on food responding in any experiment. This may reflect the fact that animals in our experiments were food restricted and that satiety signals from vagal or higher-order inputs to NTS were likely not engaged during the food

responding sessions. However, our data are in line with a recent report showing that DREADD-mediated activation of GLP-1 neurons in NTS, using similar experimental approaches described here, similarly had no effects on chow intake or body weight [34]. Also, *Glp1r* KO mice are known to consume similar amounts of chow as their wild-type counterparts [35]. These discrepancies may be explained by the fact that GLP-1 receptor agonists generally decrease cumulative chow intake when consumption is measured over relatively long time periods (2–24 h), instead of the relatively short (60 min) food responding sessions reported here, or when the food used in such experiments is high in hedonic and caloric value. Interestingly, chemogenetic stimulation of GLP-1 neurons decreases consumption of a palatable high-fat diet without altering chow intake [34] and *Glp1r* KO mice show differences in body weight when maintained on a high fat diet [36]. In light of these findings, it will be interesting to investigate the role for GLP-1 inputs to the MHb-IPN circuit in regulating palatable food consumption and long-term weight gain.

In summary, nicotine and other major drugs of abuse usurp brain reward systems otherwise dedicated to motivating the foraging and consumption of natural reinforcers such as food and water. The data reported here suggest that nicotine also recruits brain systems dedicated to avoiding natural rewards after satiety has been achieved. GLP-1 neurons are activated in response to food intake to block food reward, induce feelings of satiety and trigger meal termination. GLP-1 neurons also regulate malaise and nausea when food is consumed past satiety and contribute to anorectic responses to noxious stimuli such as lithium and cisplatin [37–48]. Analogous to feeding behavior, the present data show that GLP-1 neurons are activated by nicotine and that GLP-1 receptor transmission in the MHb-IPN circuit can abolish nicotine reward and promote avoidance. GLP-1 neurons may therefore serve as satiety sensors for nicotine that titrate intake at the levels sufficient to stimulate brain reward circuits but below those necessary to encounter aversive properties of the drug.

METHODS

Animals

Male and female mice with null mutation of the *Glp1r* gene and their wild-type littermates were bred in our animal facilities. The mutant mice had been bred for more than 10 generations onto a C57BL6/J background. Breeding was conducted by mating heterozygous pairs. All mice were housed in cages of 1–3 and were at least 6 weeks of age at the beginning of each experiment. For DREADD experiments we used commercially available 6 week-old Phox2b-Cre mice (016223, Jackson Laboratories) and Gcg-Cre mice (strain 358; MMRRC). To label GLP-1 neurons in NTS we crossed Gcg-Cre mice with commercially available ROSA-tdTom mice obtained (Stock No. 007914, Jackson Laboratories). For electrophysiological experiments we used ChAT-ChR2-YFP mice (P45-100) (014545/014546, Jackson Laboratories). To identify for neurons in NTS that express α5 nAChR subunits we used *Chrna5*-EGFP reporter mice (Stock number 030420-UCD; MMRRC). For rat self-administration and ICSS experiments, male Wistar rats weighing 275–300g were purchased from Charles River Laboratories and housed 1–2 per cage. During self-administration procedures, mice and rats were food restricted to 85–90% of their free-feeding body weight, while water was maintained without restriction. Mice and rats

were maintained in an environmentally controlled vivarium on a 12h:12h reversed light:dark cycle, and food and water were provided *ad libitum* until behavioral training commenced. Rats housed in the same cage were randomly assigned to experimental groups, and rats and mice representing each experimental group were evenly distributed among testing sessions. Whenever possible, the experimenter was blind to the experimental and/or treatment group. All animal husbandry and behavioral procedures were conducted in strict accordance with the NIH Guide for the Care and Use of Laboratory Animals and were approved by the Institutional Animal Care and Use Committees of The Scripps Research Institute and the Icahn School of Medicine at Mount Sinai.

Genotyping

Around 21 days of age, mouse pups were weaned and their tails were clipped for genetic analysis. DNA was extracted with a tissue DNA extraction kit purchased from Biomiga, Inc. (San Diego, CA). Primers for the *Glp1r* wild-type allele were: 5′-TACACAATGGGGAGCCCCTA-3′ and 5′-AAGTCATGGGATGTGTCTGGA-3′); primers for the *Glp1r* knockout allele were: 5′-CTTGGGTGGAGAGGCTATTC-3′ and 5′-AGGTGAGATGACAGGAGATC-3′. Samples were processed for genetic amplification with PCR and subsequently run on a 1% agarose gel with ethidium bromide. The band for the *Glp1r* wild-type gene was at 180 bp, and the *Glp1r* mutant gene was at 280 bp.

Drugs

For self-administration experiments in mice and rats, (-)-nicotine hydrogen tartrate salt (Sigma Chemical Co., St. Louis, MO) was dissolved in 0.9% sterile saline. All doses of nicotine refer to the free-base form. The GLP-1R antagonist Ex-9, agonist Ex-4, PKA inhibitor cAMPS-RP, and 8Br-cAMP (Tocris, Ellisville, MO) were all dissolved in 0.9% saline and microinjected at a volume of 0.5 μl for over 1 min. The injector was held in place for an additional 2 min to allow for diffusion and to prevent backflow into the cannula. Clozapine-N-oxide (CNO, Enzo Life Sciences, Farmingdale, NY) and sitagliptin (TFA salt) was diluted in 0.9% saline for intraperitoneal injection. The pH of all solutions was adjusted to ~7.4.

Virus vectors

We used commercially available adenoviral constructs (UNC vector core) for all our experiments involving infection with GFP or DREADDs. We used a non-Cre dependent M3 construct (AAV2-hSyn-HA-hM3D(Gq)-IRES-mCitrine or AAV2-hSyn-HA-hM3D(Gq)-IRES-mCherry) for non-cell specific activation of the NTS, and a non-cre dependent construct for control GFP expression (AAV2-hSyn-EGFP). To control activity of GLP-1 neurons in NTS, we used a cre dependent M3 construct (AAV2hSyn-DIO-HA-hM3D(Gq)-IRES-mCitrine). All viruses were distributed into 10 μl aliquots, kept at −80° C, and thawed immediately prior to injection. For knockdown of *Glp1r* transcripts in rat brain we used a short-hairpin (shRNA) construct that knocks down rat *Glp1r* by >80% in cultured cells and efficiently reduces *Glp1r* transcripts in rat brain (AAV1-sh-*Glp1r*-GFP; serotype 1). The sequence of the shRNA was: 5′-GATCGGGTTGCTGGTGGAAGGCGTGTATCTGTACTCAAGAGGTACAGATACACGCCTTCCACCAGCAACCTTTTTT-3′; see [49]. Knockdown of *Glp1r* in brain was confirmed

by real-time PCR using primers from ThermoFisher (Rn00562406_m1). Following injection, animals were allowed to recover for at least 2 weeks before experimentation.

Intravenous self-administration

Mice and rats were mildly food restricted to 85–90% of their free-feeding body weight and trained to press a lever in an operant chamber (Med Associates, St. Albans, VT) for food pellets (20 mg pellets for mice; 45 mg food pellets for rats; TestDiet, Richmond, IN) under a fixed-ratio 5, time out 20 sec (FR5TO20) schedule of reinforcement during 1 h daily sessions prior to catheter implantation. Once stable responding was achieved (>30 pellets per session in mice; >90 pellets per session in rats), subjects were catheterized. Mice and rats were anesthetized with an isoflurane (1–3%)/oxygen vapor mixture and prepared with intravenous catheters. Briefly, the catheters consisted of a 6 cm (mouse) or 12 cm (rat) length of silastic tubing fitted to guide cannula (Plastics One, Wallingford, CT) bent at a curved right angle and encased in dental acrylic. The catheter tubing was passed subcutaneously from the animal's back to the right jugular vein, and a 1 cm (mice) or 2.5 cm (rats) length of the catheter tip was inserted into the vein and secured with surgical silk suture. Catheters were flushed daily with physiological sterile saline solution (0.9% w/v) containing heparin (10–60 USP units/ml). Catheter integrity was tested with the ultra short-acting barbiturate anesthetic Brevital® (methohexital sodium, Eli Lilly, Indianapolis, IN). Thereafter, the animals were allowed at least 48 h to recover from surgery, then permitted to respond for food reinforcers again under the FR5TO20 schedule. Once food responding criteria was reestablished, subjects were permitted to acquire intravenous nicotine self-administration by autoshaping during 1 h daily sessions, 5–7 days per week. Nicotine was delivered through the tubing into the intravenous catheter by a Razel syringe pump (Med Associates). Each nicotine self-administration session was performed using 2 retractable levers (1 active, 1 inactive) that extended 1 cm into the chamber. Completion of the response criteria on the active lever resulted in the delivery of an intravenous nicotine infusion (0.03 ml infusion volume for mice; 0.1 ml for rats). Responses on the inactive lever were recorded but had no scheduled consequences. Animals that did not demonstrate stable responding on the training dose (at least 6 infusions per 60 min session) or showed broken IV catheters were excluded from analysis. For dose-response studies (fixed ratio schedules), animals were presented with each dose of nicotine for at least 5 days (mice) or 3 days (rats); the mean intake over the last 3 (mice) or 2 (rats) sessions for each dose was calculated and used for statistical analyses. In between each dose, subjects were placed back on the training dose for at least 2 days or until their intake returned to baseline levels before being tested on the next dose.

Microinjections, cannula and electrode implantation

Animals were anesthetized as above and positioned in a stereotaxic frame (Kopf Instruments, Tujunga, CA). Unless otherwise noted, the incisor bar was set to the 'flat-skull' position. To test the effects of NTS and GLP-1 neuronal activation on food and nicotine reinforcement, we expressed synthetic receptors (GFP control, Cre- and non Cre-dependent M3 DREADDs) in mouse NTS. In mice, two bilateral injections (0.375 μl each at a flow rate of 0.375 μl per min) were made at the following coordinates: anterior-posterior (AP) level of the occipital crest; medial-lateral (ML): μ0.5 mm from midline; dorsal-ventral (DV): −4.8

mm skull surface. To knock down *Glp1r* transcripts in MHb, rats were injected with AAV1-sh-Glp1-GFP or AAV1-GFP virus particles (titer = ~5×10^{12}) according to the following stereotaxic coordinates: flat skull, 10° angle toward midline; AP: 3.2 mm from bregma; ML: ±1.35 mm from midline; DV: −5.3 mm from skull surface. During microinjections, the injector needles extended into MHb and virus particles were administered in a volume of 0.3 μL and at a rate of 0.1 μL per minute. The injector needle remained in place for 2 min post-injection. For IPN microinjections in rats, guide cannulae (Plastics One, Wallingford, CT) were implanted as follows: (flat skull; 10° angle toward midline; AP: −6.72 mm from bregma; ML: ±1.6 mm from midline; DV: −6.5 mm from brain surface). During injections, the injector needles extended 2 mm below the tip of the cannula for placement into the brain region and were administered at a volume of 0.5 μl and rate of 0.5 μl per min. The injector needle remained in place for a minimum of 2 min post-injection. For the ICSS electrode, a stainless steel bipolar electrode (Plastics One) was implanted into the lateral hypothalamus (AP: −0.5 mm from bregma; ML: ±1.7 mm from midline; DV: −8.3 mm from brain surface; incisor bar was adjusted to 5 mm above the interaural line).

ICSS Procedure

Rats were trained to respond according to a modification of the discrete-trial current-threshold procedure of Kornetsky and Esposito [22] in an operant box equipped with a wheel manipulandum and ICSS stimulator (Med Associates). Briefly, a trial was initiated by the delivery of a non-contingent electrical stimulus. This electrical reinforcer had a duration of 500 ms and consist of 0.1 ms rectangular cathodal pulses that delivered at a frequency of 50–100 Hz. The frequency of the stimulation was selected for individual rats so that threshold elevation and lowering may be detected, and this frequency was held constant throughout the experiment. A one-quarter turn of the wheel manipulandum within 7.5 sec of the delivery of the non-contingent stimulation resulted in the delivery of an electrical stimulus identical in all parameters to the non-contingent stimulus that initiated the trial. After a variable inter-trial interval (7.5–12.5 sec, mean of 10 sec), another trial was initiated with the delivery of a non-contingent electrical stimulus. Failure to respond to the non-contingent stimulus within 7.5 sec resulted in the onset of the inter-trial interval. Responding during the inter-trial interval delayed the onset of the next trial by 12.5 sec. In each testing session, current levels were varied in alternating descending (x2) and ascending (x2) series in 5 μA steps. A set of five trials was presented for each current intensity. The threshold for each series is defined as the midpoint between two consecutive current intensities that yield “positive scores” (animals respond for at least three of the five trials) and two consecutive current intensities that yield “negative scores” (animals do not respond for three or more of the five trials). The overall threshold for the session is defined as the mean of the thresholds for the four individual series. Threshold data are presented as percent of baseline values due to inter-subject variability in baseline rates.

Tissue dissection

Mice and rats were euthanized by inhalation of CO_2, brains were rapidly removed, and frozen on dry ice. Tissues were stored at −80°C until dissection. Brains were sliced on a cryostat, and bilateral dissections were made for the hippocampus, habenula, NTS, IPN

and/or VTA with a scalpel. Samples were pooled across multiple subjects due to the small size of selected brain areas and stored in at −80°C until processing.

Brain Perfusion and Fixation

Mice and rats were anesthetized with sodium pentobarbital (0.1 mg/10 g body weight) and perfused through the ascending aorta with 0.9% saline, followed by 4% paraformaldehyde in 0.1 M phosphate buffer saline (PBS; pH 7.4). Brains were harvested, postfixed overnight in 4% paraformaldehyde, and then stored in 30% sucrose in 0.1 M phosphate buffer (pH 7.4) for 72h. All brains were cut into 30–40 μm coronal sections on a cryostat, and the floating sections were stored in 0.1 M PBS with 0.01% sodium azide at 4°C until processing for immunohistochemistry.

Fluorescence Immunolabeling

Floating sections were processed for fluorescent immunostaining of GFP, GLP-1, TH and Fos. To localize mCitrine- or GFP-tagged cells in mice, we used a chicken polyclonal IgG that recognizes a 27 kDa protein derived from the jellyfish *Aequorea Victoria*. Sections were rinsed in 0.1 M PBS, pH 7.4, with 0.5% Triton-X 100 (PBT) and then blocked in 10% normal donkey serum/PBT for 1 h. Thereafter, sections were incubated in the primary antibody in PBT at 4 °C overnight (incubation for GLP-1 was 72 h). The primary antibodies were diluted as follows: chicken anti-GFP (1:1500; ab-13970, AbCam), rabbit anti-GLP-1 (1:1200; T4057, Bachem, Torrance, CA), mouse anti-TH (1:500, SC-25269, Santa Cruz, Santa Cruz, CA), and rabbit anti-Fos (1:1500, ab-7963, AbCam, Cambridge, MA). On day 2, the sections were rinsed and incubated in two of the following antibodies: Alexa 488 donkey anti-rabbit (1:500, A21206, Invitrogen, Carlsbad, CA), Alexa 488 donkey anti-mouse (1:500, R37114, Invitrogen), Alexa 594 donkey anti-rabbit (1:500, A21207, Invitrogen), Alexa 488 donkey anti-mouse (1:500, R37115 Invitrogen), or DyLight 488 donkey anti-chicken (1:400, 703-485-155, Jackson ImmunoResearch, West Grove, PA). Sections were incubated with secondary antibodies in PBS (in 2% donkey serum) for 2 h. Next, the sections were rinsed, mounted on slides with VectaShield (with DAPI) (H-1200, Vector Labs, Burlingame, CA), and coverslipped. Controls included processing the secondary antibodies alone to verify background staining, processing each primary with the secondary antibody to verify laser-specific excitation, examining for autofluorescence in an alternate laser channel with tissue lacking that laser-specific probe, and using sequential scanning. For subsequent fluorescent images, only brightness and/or contrast levels were adjusted post-acquisition and were imposed across the entire image. All antibodies used have been previously validated for the intended applications, as per manufacturer. For all representative images of qualitative data, the immunolabeling experiment was successfully repeated in at least 3 animals.

Fos Procedure

90 min after saline, nicotine or CNO injections, animals were perfused and brain removed and stored as described above. Brain sections were cut at 40 μm on a cryostat and stored in 0.1 M PBS with 0.01 % sodium azide until processing. For Fos immunolabeling, sections were rinsed in 0.1 M PBS (pH 7.4), treated with 0.3% H_2O_2-PBS for 15 min, rinsed in PBS, and then blocked in 10 % normal goat serum and 0.5% Triton X-100 in PBS for 1 hr.

Thereafter, sections were incubated in rabbit anti-Fos IgG (1:3000 dilution; Abcam,) in 0.5 % Triton-PBS overnight at 4°C. The following day, sections were incubated at room temperature for 2 h, rinsed in PBS, and then incubated in 1:300 dilution of goat anti-rabbit secondary IgG (BA-1000, Vector Labs) in 0.5% Triton X-100 in PBS for 2 h. Following rinsing, sections were incubated in ABC Elite (PK-6100, Vector Labs) for 90 min, rinsed in PBS, and immunoreactivity was revealed by using 3-diaminobenzidine (DAB) with nickel (SK-4100, Vector Labs). To reduce variability in the background and to standardize the staining, sections from subjects across groups were processed concurrently. Sections were mounted and coverslipped with Permount (Fisher Scientific, Waltham, MA). Fos-immunoreactive cells in the IPN were counted for each animal under 20X magnification. The number of Fos-immunoreactive cells in IPN section was added and then divided by the number of IPN sections for that given animal (average 6–8 sections), yielding an individual animal average. All representative Fos images were taken from animals receiving the indicated treatment and were also used for quantification.

Electrophysiology

Before decapitation, ChAt-ChR2-YFP mice (P45-100) were briefly anesthetized with isoflurane and subsequently transcardially perfused with 4°C NMDG solution (in mM) 135 N-Methyl-D-glucamine (NMDG), 1 KCl, 1.2 KH_2PO_4, 1.5 $MgCl_2$, 0.5 $CaCl_2$, 20 choline bicarbonate, 10 glucose and 295–305 mOsm, equilibrated with 95% O_2/5% CO_2. The mouse was decapitated, the brain was removed and glued to a block and sliced using a Leica VT1200s vibratome in 4°C NMDG solution. Coronal slices of 250 μm thickness were cut such that the preparation contained the IPN and then submerged in 36°C oxygenated standard artificial cerebral spinal fluid ACSF (in mM): 119 NaCl, 2.5 KCl, 1.0 NaH_2PO_4, 26.2 $NaHCO_3$, 1.3 $MgCl_2$, 2.5 $CaCl_2$, 11 glucose and 285–290 mOsm, equilibrated with 95% O_2/5% CO_2) for 30 mins and then stored at room temperature with constant oxygenation until being transferred to the recording chamber.

Standard whole-cell voltage-clamp recordings were made using a MultiClamp 700B amplifier and a Digidata 1440A digitizer (Molecular Devices) through borosilicate glass electrodes (3–5 MΩ), filtered at 2.6–3 kHz and digitized at 20 kHz using Clampex 10.3 software (Molecular Devices). For all recordings, series resistance was 8 to 14 MΩ and was left uncompensated. Series resistance was monitored continuously during all recordings, and a change beyond 15 % was not accepted for data analysis.

Voltage-clamp recordings were used to measure miniature excitatory postsynaptic currents (mEPSCs) and evoked excitatory postsynaptic currents. During recordings, slices were superfused with aCSF, containing picrotoxin (100 μm), that was heated to 29 – 33°C by passing the solution through a feedback-controlled in-line heater (Warner Instruments, Hamden, CT) before entering the chamber. Recordings were made under visual guidance (40x, differential interference contrast optics) using a Scientifica SliceScope Pro 6000 (Scientifica, UK). For recordings, the membrane potential was held at −70 mV. Patch pipettes were filed with a cesium-based solution (in mM): 140 cesium methanesulfonate, 5 TEA-Cl, 0.4 EGTA, 20 HEPES, 2.5 Mg-ATP, 0.25 Na-GTP, 1 QX-314, pH 7.3 and 290

mOsm. Cells were identified within the IPN, ChAt-ChR2 was verified by visualizing the YFP signal.

For miniature recordings, once a cell was patched the perfusion was switched to ACSF containing TTX (1 μM) using the Programmable Perfusion System (Scientifica, UK). Cells were allowed to stabilize after starting toxin-containing solutions for at least 10 mins. Due to possible effects of action potential blockade on synaptic properties, all mEPSC recordings were made within 30 mins after TTX was applied to the slice. Once a baseline was recorded (~5 mins) the perfusion system was switched again to ACSF containing TTX (1 μM) and Exendin-4 (100 nM). For miniature event analysis, at least 50 seconds of events were analyzed from each cell and each condition using Clampfit 10.3 (Molecular Devices). The event threshold was set at 10 pA and the baseline amplitude was adjusted for each event to midsignal at the initiation time of event.

For evoked EPSC recordings, all evoked responses were delivered using a SLOC laser (Shanghai Laser and Optics Century Co., Shanghai, China) at 473 nM, through an 105 μm optic fiber lowered into the bath just above the slice. The duration of the pulse was 1–2 ms, ~10 mW2. Once a stable evoked response was achieved, a baseline was recorded (~5 mins) then the perfusion was switched to ACSF containing Exendin-4 (100 nM) and evoked responses were recorded for 10–20 mins. Amplitudes of EPSCs were calculated using Clampfit 10.3 (Molecular Devices) by averaging 15–50 EPSCs by measuring the peak (5 ms window) compared to the baseline (10 ms window). TTX and Exendin-4 were purchased from Tocris Bioscience. All other chemicals were purchased from Sigma-Aldrich.

Statistical Analyses

Animal sample size was justified by previously published data or preliminary experiments. Data distribution was assumed to be normal but this was not formally tested. For all experiments animals (with the same genotype) were randomly allocated to experimental groups. For self-administration experiments, animals that did not achieve stable levels of intake (<20 % variation in intake across three consecutive days), or that took less than <5 nicotine infusions on average across sessions were excluded from experiments. All data were analyzed by one- or two-way analysis of variance (ANOVA) or t-test using Graphpad Prism software (La Jolla, CA). Significant main or interaction effects were followed by Bonferroni or Newman-Keuls post-hoc tests as appropriate. The criterion for significance was set at $p<0.05$. For all electrophysiological data, results are shown as the mean ± SEM. When appropriate, Grubbs test was used to identify outliers. The data that support the findings of this study are available from the corresponding author upon reasonable request.

Supplementary Material

Refer to Web version on PubMed Central for supplementary material.

Acknowledgments

This work was supported by the US National Institutes of Health (DA032225 to L.M.T.; DK096139 to M.R.H.; DA020686 to P.J.K.).

References

1. Kenny PJ, Markou A. Nicotine self-administration acutely activates brain reward systems and induces a long-lasting increase in reward sensitivity. Neuropsychopharmacology : official publication of the American College of Neuropsychopharmacology. 2006; 31:1203–1211. [PubMed: 16192981]
2. Picciotto MR, et al. Acetylcholine receptors containing the beta2 subunit are involved in the reinforcing properties of nicotine. Nature. 1998; 391:173–177. [PubMed: 9428762]
3. Russell MA, Wilson C, Patel UA, Feyerabend C, Cole PV. Plasma nicotine levels after smoking cigarettes with high, medium, and low nicotine yields. British medical journal. 1975; 2:414–416. [PubMed: 1168517]
4. Fowler CD, Kenny PJ. Nicotine aversion: Neurobiological mechanisms and relevance to tobacco dependence vulnerability. Neuropharmacology. 2014; 76(Pt B):533–544. [PubMed: 24055497]
5. Grill HJ, Hayes MR. Hindbrain neurons as an essential hub in the neuroanatomically distributed control of energy balance. Cell metabolism. 2012; 16:296–309. [PubMed: 22902836]
6. Jensen KP, et al. A CHRNA5 Smoking Risk Variant Decreases the Aversive Effects of Nicotine in Humans. Neuropsychopharmacology : official publication of the American College of Neuropsychopharmacology. 2015; 40:2813–2821. [PubMed: 25948103]
7. Goke R, Larsen PJ, Mikkelsen JD, Sheikh SP. Distribution of GLP-1 binding sites in the rat brain: evidence that exendin-4 is a ligand of brain GLP-1 binding sites. The European journal of neuroscience. 1995; 7:2294–2300. [PubMed: 8563978]
8. Dalle S, Burcelin R, Gourdy P. Specific actions of GLP-1 receptor agonists and DPP4 inhibitors for the treatment of pancreatic beta-cell impairments in type 2 diabetes. Cellular signalling. 2013; 25:570–579. [PubMed: 23159576]
9. Egecioglu E, Engel JA, Jerlhag E. The glucagon-like peptide 1 analogue, exendin-4, attenuates the rewarding properties of psychostimulant drugs in mice. PloS one. 2013; 8:e69010. [PubMed: 23874851]
10. Graham DL, Erreger K, Galli A, Stanwood GD. GLP-1 analog attenuates cocaine reward. Molecular psychiatry. 2013; 18:961–962. [PubMed: 23089631]
11. Shirazi RH, Dickson SL, Skibicka KP. Gut peptide GLP-1 and its analogue, Exendin-4, decrease alcohol intake and reward. PloS one. 2013; 8:e61965. [PubMed: 23613987]
12. Campos RV, Lee YC, Drucker DJ. Divergent tissue-specific and developmental expression of receptors for glucagon and glucagon-like peptide-1 in the mouse. Endocrinology. 1994; 134:2156–2164. [PubMed: 8156917]
13. Scott MM, Williams KW, Rossi J, Lee CE, Elmquist JK. Leptin receptor expression in hindbrain Glp-1 neurons regulates food intake and energy balance in mice. The Journal of clinical investigation. 2011; 121:2413–2421. [PubMed: 21606595]
14. Mastitskaya S, et al. Cardioprotection evoked by remote ischaemic preconditioning is critically dependent on the activity of vagal pre-ganglionic neurones. Cardiovascular research. 2012; 95:487–494. [PubMed: 22739118]
15. Kang BJ, et al. Central nervous system distribution of the transcription factor Phox2b in the adult rat. The Journal of comparative neurology. 2007; 503:627–641. [PubMed: 17559094]
16. Fowler CD, Kenny PJ. Intravenous nicotine self-administration and cue-induced reinstatement in mice: effects of nicotine dose, rate of drug infusion and prior instrumental training. Neuropharmacology. 2011; 61:687–698. [PubMed: 21640128]
17. Ren J, et al. Habenula “cholinergic” neurons co-release glutamate and acetylcholine and activate postsynaptic neurons via distinct transmission modes. Neuron. 2011; 69:445–452. [PubMed: 21315256]
18. Gorlich A, et al. Reexposure to nicotine during withdrawal increases the pacemaking activity of cholinergic habenular neurons. Proc Natl Acad Sci U S A. 2013; 110:17077–17082. [PubMed: 24082085]
19. Ban K, et al. Cardioprotective and vasodilatory actions of glucagon-like peptide 1 receptor are mediated through both glucagon-like peptide 1 receptor-dependent and -independent pathways. Circulation. 2008; 117:2340–2350. [PubMed: 18427132]

20. McGehee DS, Heath MJ, Gelber S, Devay P, Role LW. Nicotine enhancement of fast excitatory synaptic transmission in CNS by presynaptic receptors. Science. 1995; 269:1692–1696. [PubMed: 7569895]
21. Fowler CD, Kenny PJ. Nicotine aversion: Neurobiological mechanisms and relevance to tobacco dependence vulnerability. Neuropharmacology. 2013
22. Kornetsky C, Esposito RU, McLean S, Jacobson JO. Intracranial self-stimulation thresholds: a model for the hedonic effects of drugs of abuse. Arch Gen Psychiatry. 1979; 36:289–292. [PubMed: 420547]
23. Markou A, Koob GF. Construct validity of a self-stimulation threshold paradigm: effects of reward and performance manipulations. Physiol Behav. 1992; 51:111–119. [PubMed: 1741436]
24. Kenny PJ. Brain reward systems and compulsive drug use. Trends in pharmacological sciences. 2007; 28:135–141. [PubMed: 17276521]
25. Schaefer GJ, Michael RP. Task-specific effects of nicotine in rats. Intracranial self-stimulation and locomotor activity. Neuropharmacology. 1986; 25:125–131. [PubMed: 3703168]
26. Sartor CE, et al. Initial response to cigarettes predicts rate of progression to regular smoking: findings from an offspring-of-twins design. Addictive behaviors. 2010; 35:771–778. [PubMed: 20385446]
27. Norton GR, Barske B. The role of aversion in the rapid-smoking treatment procedure. Addictive behaviors. 1977; 2:21–25. [PubMed: 848373]
28. Merchenthaler I, Lane M, Shughrue P. Distribution of pre-pro-glucagon and glucagon-like peptide-1 receptor messenger RNAs in the rat central nervous system. The Journal of comparative neurology. 1999; 403:261–280. [PubMed: 9886047]
29. Nishikawa T, Fage D, Scatton B. Evidence for, and nature of, the tonic inhibitory influence of habenulointerpeduncular pathways upon cerebral dopaminergic transmission in the rat. Brain research. 1986; 373:324–336. [PubMed: 2424555]
30. Fowler CD, Lu Q, Johnson PM, Marks MJ, Kenny PJ. Habenular alpha5 nicotinic receptor subunit signalling controls nicotine intake. Nature. 2011; 471:597–601. [PubMed: 21278726]
31. Fowler CD, Tuesta L, Kenny PJ. Role of alpha5* nicotinic acetylcholine receptors in the effects of acute and chronic nicotine treatment on brain reward function in mice. Psychopharmacology. 2013
32. Miranda MI, Bermudez-Rattoni F. Reversible inactivation of the nucleus basalis magnocellularis induces disruption of cortical acetylcholine release and acquisition, but not retrieval, of aversive memories. Proceedings of the National Academy of Sciences of the United States of America. 1999; 96:6478–6482. [PubMed: 10339613]
33. van Bloemendaal L, Ten Kulve JS, la Fleur SE, Ijzerman RG, Diamant M. Effects of glucagon-like peptide 1 on appetite and body weight: focus on the CNS. J Endocrinol. 2014; 221:T1–16. [PubMed: 24323912]
34. Wang XF, et al. Endogenous Glucagon-like Peptide-1 Suppresses High-Fat Food Intake by Reducing Synaptic Drive onto Mesolimbic Dopamine Neurons. Cell reports. 2015; 12:726–733. [PubMed: 26212334]
35. Scrocchi LA, Drucker DJ. Effects of aging and a high fat diet on body weight and glucose tolerance in glucagon-like peptide-1 receptor −/− mice. Endocrinology. 1998; 139:3127–3132. [PubMed: 9645685]
36. Ayala JE, et al. Glucagon-like peptide-1 receptor knockout mice are protected from high-fat diet-induced insulin resistance. Endocrinology. 2010; 151:4678–4687. [PubMed: 20685876]
37. Bello NT, Moran TH. GLP-1 agonists and satiety. Immunology, Endocrine & Metabolic Agents in Medicinal Chemistry. 2008; 8:311–316.
38. Gutzwiller JP, et al. Glucagon-like peptide-1: a potent regulator of food intake in humans. Gut. 1999; 44:81–86. [PubMed: 9862830]
39. Garcia-Diaz DE, Jimenez-Montufar LL, Guevara-Aguilar R, Wayner MJ, Armstrong DL. Olfactory and visceral projections to the nucleus of the solitary tract. Physiol Behav. 1988; 44:619–624. [PubMed: 3237848]
40. Scott TR, Yaxley S, Sienkiewicz ZJ, Rolls ET. Gustatory responses in the nucleus tractus solitarius of the alert cynomolgus monkey. J Neurophysiol. 1986; 55:182–200. [PubMed: 3950684]

41. Hayama T, Ito S, Ogawa H. Responses of solitary tract nucleus neurons to taste and mechanical stimulations of the oral cavity in decerebrate rats. Exp Brain Res. 1985; 60:235–242. [PubMed: 4054268]

42. Chang FC, Scott TR. Conditioned taste aversions modify neural responses in the rat nucleus tractus solitarius. J Neurosci. 1984; 4:1850–1862. [PubMed: 6737042]

43. Qin C, Sun Y, Chen JD, Foreman RD. Gastric electrical stimulation modulates neuronal activity in nucleus tractus solitarii in rats. Auton Neurosci. 2005; 119:1–8. [PubMed: 15893702]

44. Schwartz GJ. The role of gastrointestinal vagal afferents in the control of food intake: current prospects. Nutrition. 2000; 16:866–873. [PubMed: 11054591]

45. Appleyard SM, et al. Visceral afferents directly activate catecholamine neurons in the solitary tract nucleus. J Neurosci. 2007; 27:13292–13302. [PubMed: 18045923]

46. Monnikes H, Lauer G, Arnold R. Peripheral administration of cholecystokinin activates c-fos expression in the locus coeruleus/subcoeruleus nucleus, dorsal vagal complex and paraventricular nucleus via capsaicin-sensitive vagal afferents and CCK-A receptors in the rat. Brain research. 1997; 770:277–288. [PubMed: 9372230]

47. Willing AE, Berthoud HR. Gastric distension-induced c-fos expression in catecholaminergic neurons of rat dorsal vagal complex. Am J Physiol. 1997; 272:R59–67. [PubMed: 9038991]

48. Rinaman L, Baker EA, Hoffman GE, Stricker EM, Verbalis JG. Medullary c-Fos activation in rats after ingestion of a satiating meal. Am J Physiol. 1998; 275:R262–268. [PubMed: 9688987]

49. Schmidt HD, et al. Glucagon-Like Peptide-1 Receptor Activation in the Ventral Tegmental Area Decreases the Reinforcing Efficacy of Cocaine. Neuropsychopharmacology. 2016; 41:1917–1928. [PubMed: 26675243]

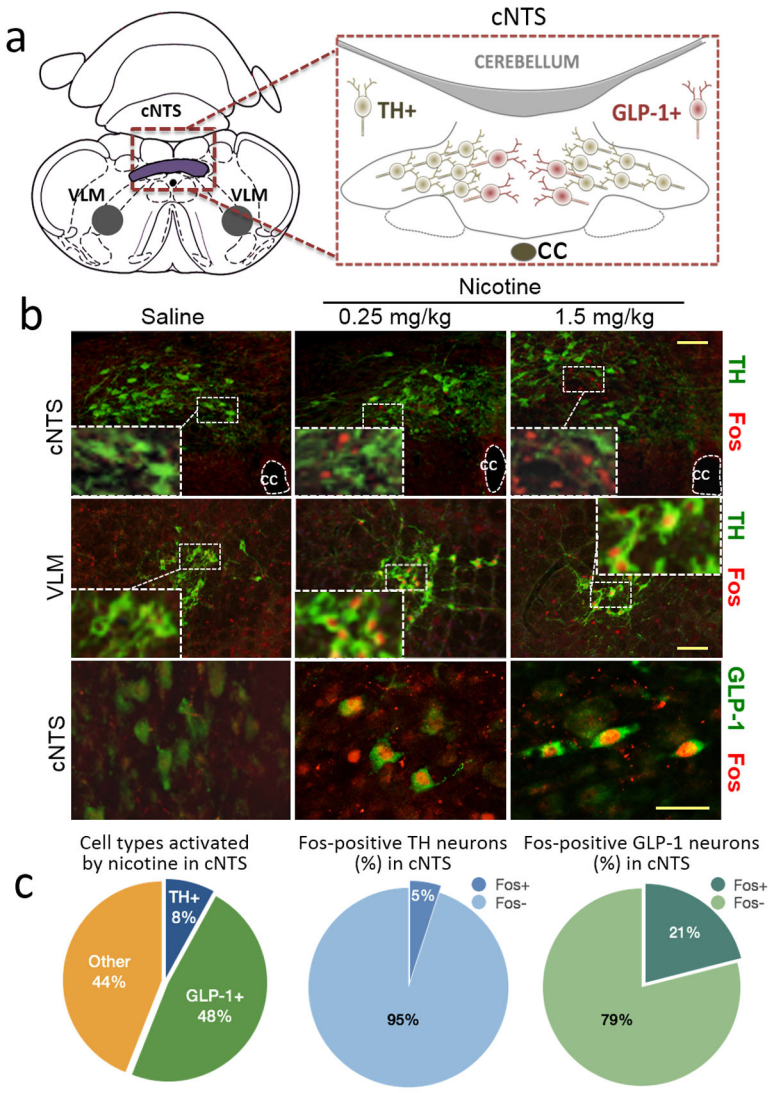

Figure 1. Nicotine activates medullary GLP-1 neurons

(a) Graphical representation of GLP-1-positive (GLP-1+) and tyrosine hydroxylase-positive (TH+) neurons in the cNTS (cc: central canal). **(b)** Representative micrographs of Fos (in red) and GLP-1+ or TH+ (in green) neurons in the cNTS and VLM after saline or nicotine (0.25–1.5 mg/kg) injection (insert: 20x magnification of marked area). **(c)** Relative neuronal recruitment by cell type in cNTS following nicotine challenge. Scale bar, 100μm.

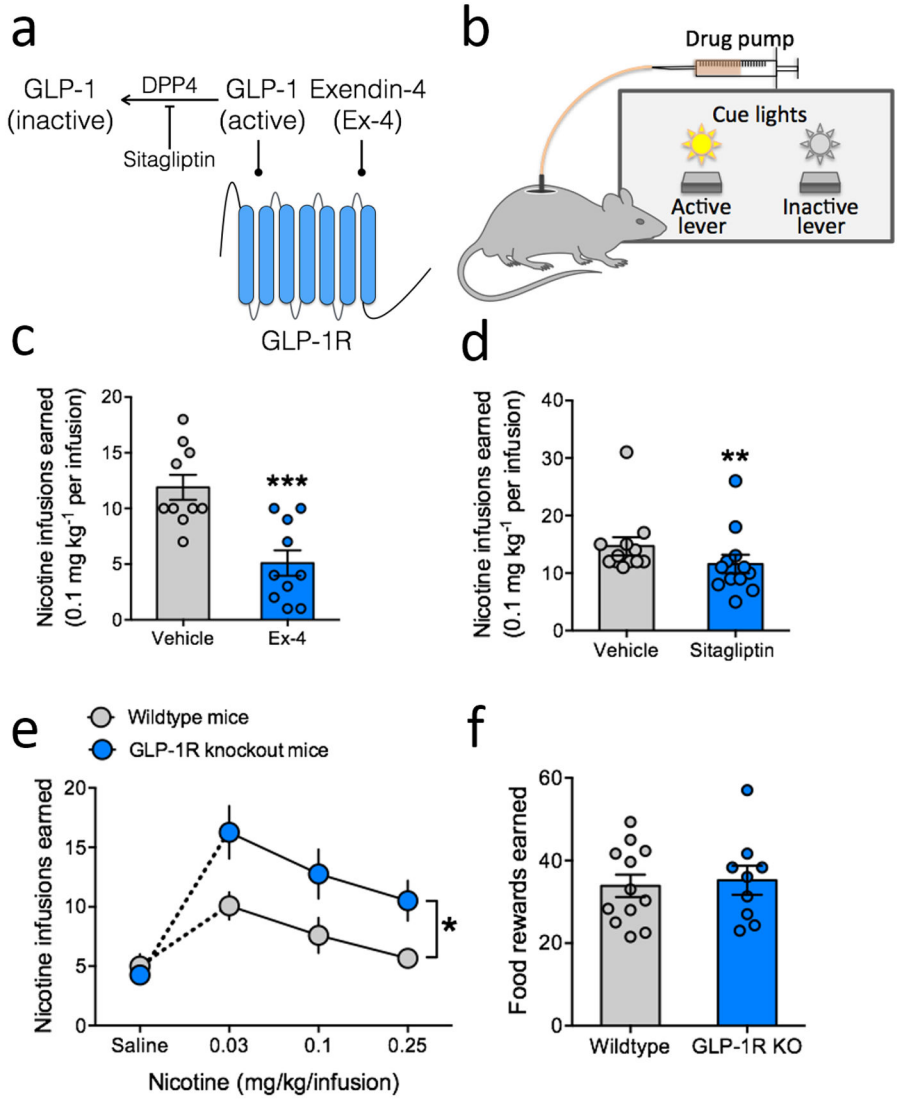

Figure 2. GLP-1 regulates nicotine intake

(a) Graphical representation of mechanisms of GLP-1 receptor (GLP-1R) activation by sitagliptin and exendin-4 (Ex-4). **(b)** Graphical representation of intravenous nicotine self-administration procedure. **(c)** Mean (± s.e.m.) number of nicotine infusions earned by mice after Ex-4 (10 μg/kg) administration. ***P<0.001, paired t-test (n=10). **(d)** Mean (± s.e.m.) number of nicotine infusions earned by mice after sitagliptin administration. **P<0.01, paired t-test (n=12). **(e)** Nicotine dose-response curve of GLP-1R knockout (n=8) and wild-type (n=6) mice. Data points represent mean (± s.e.m.) number of infusions earned at each nicotine dose. Two-way repeated-measures (RM) ANOVA, Genotype: $F_{(1, 12)}$=6.29, *p<0.05; Nicotine: $F_{(2, 24)}$=9.49, p<0.001; Genotype × Nicotine: $F_{(2, 24)}$=0.18, NS. **(f)** Mean (± s.e.m.) number of food rewards earned during 1-hour operant training sessions between GLP-1R knockout (n=9) and wild-type (n=12) mice. Scale bar, 100 μm.

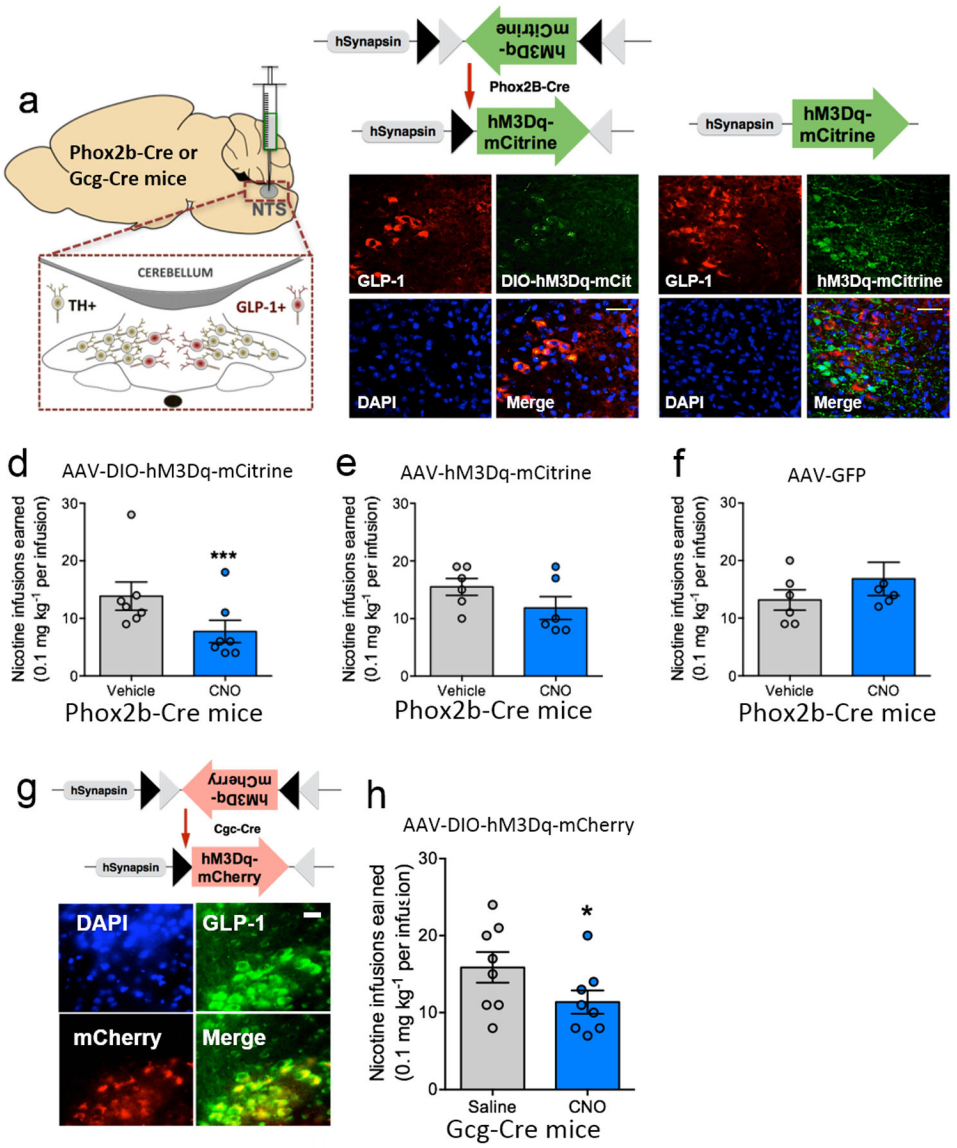

Figure 3. Chemogenetic activation of GLP-1 neurons mice decreases nicotine intake

(a) Graphical representation of NTS and the site of stereotaxic DREADD virus injections in Phox2b-Cre of Gcg-Cre mice. **(b)** Upper panel: DIO vector design and selective expression in Phox2b-Cre neurons. Lower panel: Representative micrograph showing selective expression of AAV-DIO-hM3Dq-mCitrine vector in GLP-1-immunopositive neurons in Phox2b-Cre mice. **(c)** Non-DIO vector design (upper panel) and representative micrograph showing non-specific expression throughout cNTS neurons in Phox2b-Cre mice (lower panel). **(d)** Mean (± s.e.m.) number of nicotine infusions after saline or CNO (1 mg/kg, IP) injection in Phox2b-Cre mice expressing DIO-hM3Dq. *P=0.0032, paired t-test; n=6. **(e)** Mean (± s.e.m.) number of nicotine infusions after saline or CNO injection to Phox2b-Cre mice expressing hM3Dq (n=5). P=0.0660, paired t-test. **(f)** Mean (± s.e.m.) number of nicotine infusions after saline or CNO injection in Phox2b-Cre mice expressing AAV-EGFP vector (n=5). P=0.2643, paired t-test. **(g)** Upper panel: DIO vector design. Lower panel:

Representative micrograph showing selective expression of AAV-DIO-hM3Dq-mCherry in GLP-1-immunopositive neurons of Gcg-Cre mice. **(h)** Mean (± s.e.m.) number of nicotine infusions after saline or CNO (3 mg/kg, IP) injection in Gcg-Cre mice expressing FLEX-hM3Dq. *P=0.0011, paired t-test; *n*=8.

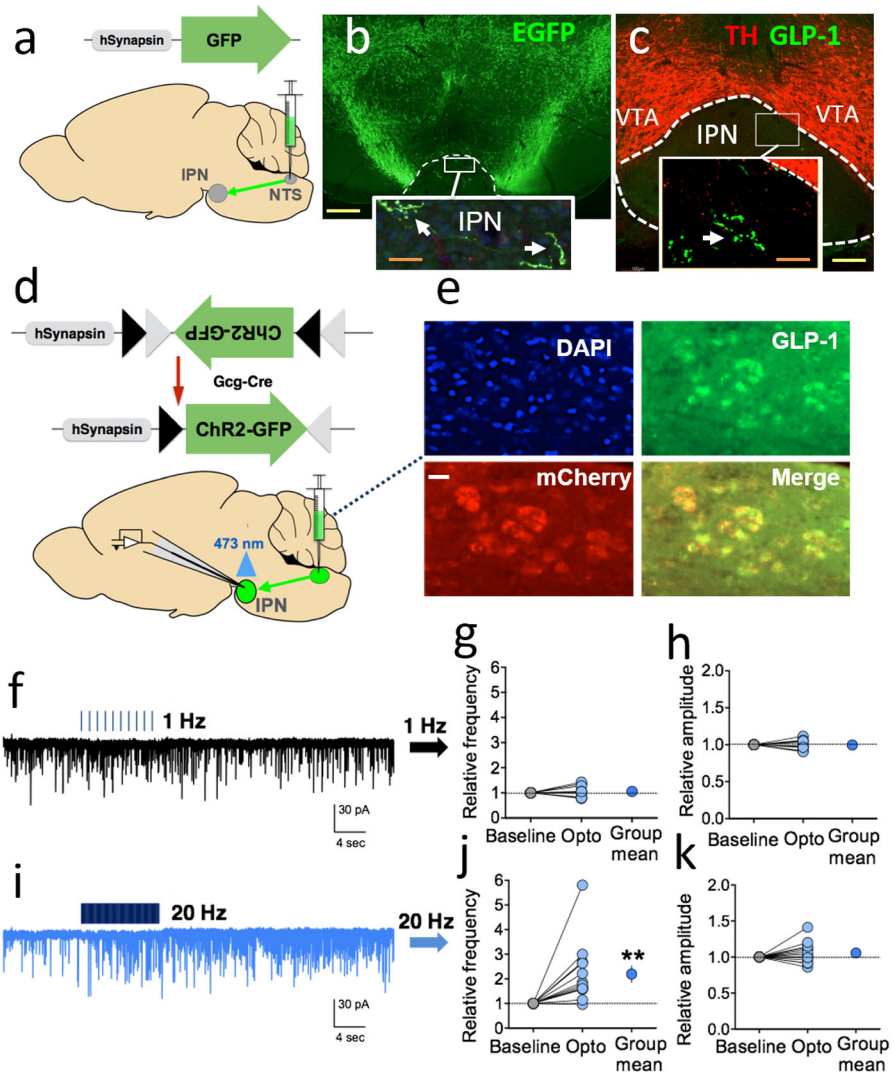

Figure 4. GLP-1 inputs from NTS stimulate IPN neurons

(a) Graphical representation of AAV-EGFP injection into the mouse cNTS and projection of NTS neurons to IPN. **(b)** Midbrain micrograph following cNTS AAV-EGFP injection. Insert shows cNTS-to-IPN projections (in green; identified by white arrows). **(c)** Micrograph of IPN showing GLP-1 immunoreactive fibers in IPN (green) and surrounding VTA identified by TH immunoreactivity (red). Insert shows GLP-1+ fiber in IPN (identified by white arrow). **(d)** Upper panel: DIO-ChR2-GFP vector design. Lower panel: Graphical representation of site of DIO-ChR2-GFP injection into NTS. **(e)** Representative micrographs showing expression of AAV-DIO-ChR2-GFP in GLP-1-immunopositive neurons. **(f)** Representative micrographs showing expression of GFP+ fibers in IPN. **(g)** Example traces of currents evoked by 1 Hz optical stimulation in IPN neurons. **(h)** Summarized results (mean ± s.e.m.) of changes in relative frequency of excitatory currents in IPN neurons by 1 Hz optical stimulation. **(i)** Summarized results (mean ± s.e.m.) of changes in relative amplitude of excitatory currents in IPN neurons by 1 Hz optical stimulation. **(j)** Example traces of currents evoked by 20 Hz optical stimulation in IPN neurons. **(k)** Summarized

results (mean ± s.e.m.) of changes in relative frequency of excitatory currents in IPN neurons by 20 Hz optical stimulation. **(l)** Summarized results (mean ± s.e.m.) of changes in relative amplitude of excitatory currents in IPN neurons by 20 Hz optical stimulation. Yellow scale bar, 100μm; orange scale bar, 25 μm.

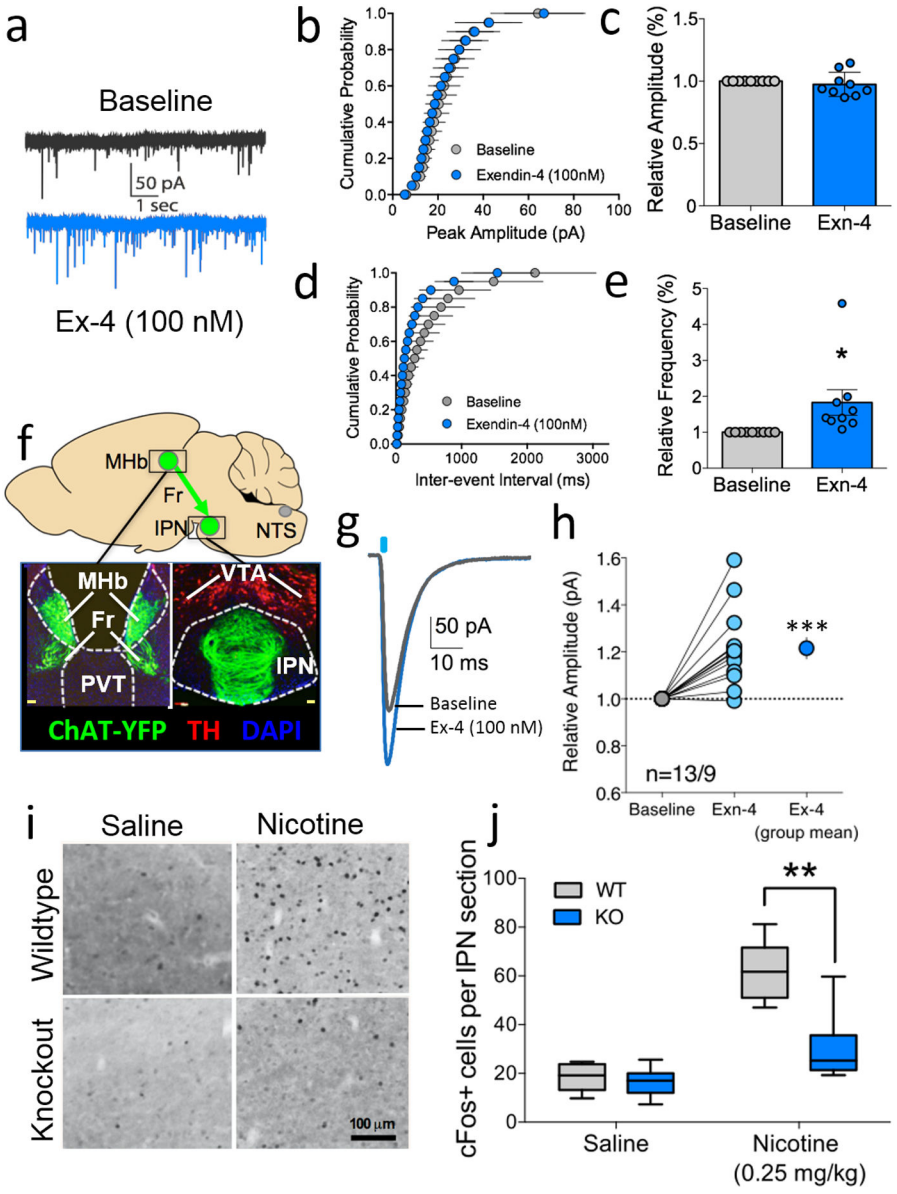

Figure 5. GLP-1 activates IPN neurons by stimulating habenular terminals

(a) Graphical in IPN neurons before and after bath application of Ex-4 (100 nM). **(b)** Cumulative probability **(c)** and summarized results (mean ± s.e.m.) showing that the relative amplitude of mEPSCs in IPN neurons is not altered by Ex-4. **(d)** Cumulative probability **(e)** and summarized results (mean ± s.e.m.) showing that the relative frequency of mEPSCs in IPN neurons is increased by Ex-4. *P<0.05, paired t-test; *n*=9 cells from 4 animals. **(f)** Graphical representation the MHb-IPN circuit (green). Micrographs below: Cholinergic MHb neurons (left) send axonal projections to the IPN (right) as evidenced by fluorescence from ChAT-ChR2-eYFP mice. Nuclear DAPI staining is shown in blue. (**g**) Sample trace showing that the amplitude of light-evoked EPSCs in IPN neurons from ChAT-ChR2-eYFP mice is increased by Ex-4. (**h**) Summarized results showing that Ex-4 significantly increases the amplitude of light-evoked EPSC in IPN neurons. ***P<0.001, paired t-test; *n*=13 cells

from 9 cells animals. **(i)** Representative micrographs showing induction of Fos in IPN following nicotine challenge in GLP-1R KO and wild-type mice. **(j)** Mean (± s.e.m.) number of Fos-positive neurons per IPN section in GLP-1R knockout (saline, n=6; nicotine, n=7) and wild-type (saline, n=6; nicotine, n=7) mice following nicotine challenge. Two-way ANOVA, Genotype: $F_{(1, 22)}$=17.69, p=0.0004; Nicotine: $F_{(1, 22)}$=51.71, p<0.0001; Genotype × Nicotine: $F_{(1, 10)}$=13.36, **p=0.0014.

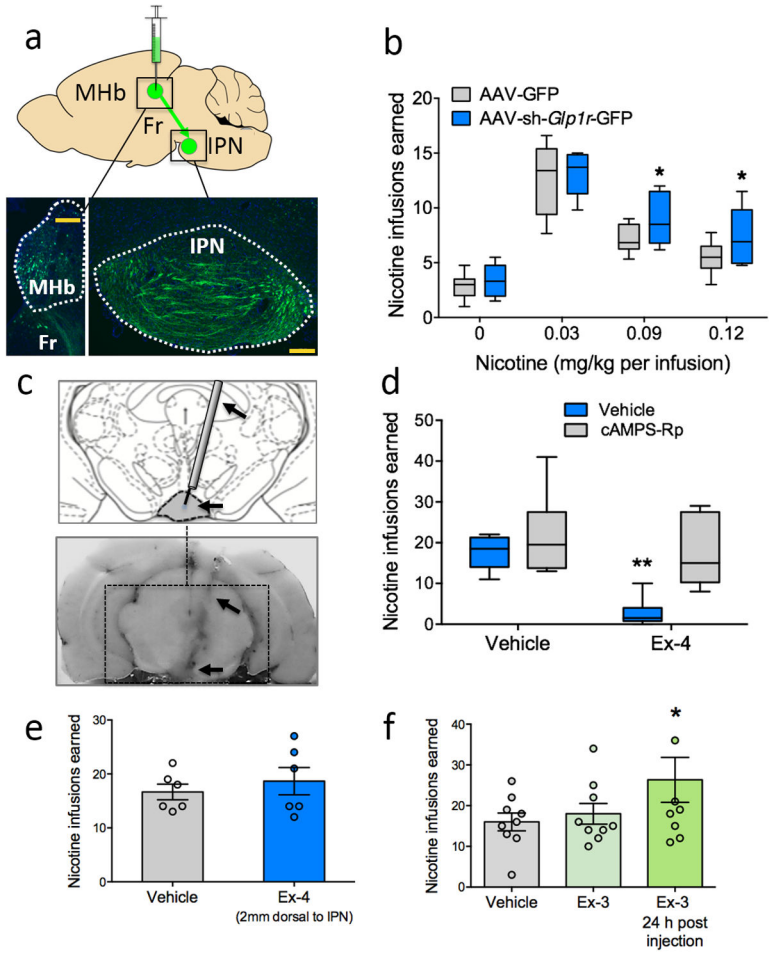

Figure 6. GLP-1 transmission in IPN regulates nicotine intake

(a) Graphical representation the MHb-IPN circuit (green) and targeting of AAV-sh-*Glp1r*-GFP or AAV-GFP viruses into MHb. Micrographs below: GFP+ neurons in MHb neurons and GFP+ fibers in the fasciculus retroflexus (Fr) (left) and GFP+ terminals (right) in virus-treated rats. **(b)** Mean (± s.e.m.) number of nicotine infusions in AAV-GFP and AAV-sh-*Glp1r*-GFP rats. *P<0.05, post-hoc test after main effect in two-way ANOVA between intake at the higher nicotine doses (0.09, 0.12 mg kg^{-1} per infusion); n=6–7 per group). **(c)** Graphical representation of indwelling cannula directed toward IPN for microinjection (upper panel) and photograph showing representative cannula tract (identified by black arrows) in rat included in study (lower panel). **(d)** Mean (± s.e.m.) number of nicotine infusions earned after IPN infusion of vehicle (saline) or Ex-4 (0.1μg/0.5 μl) in rats (n=6) pre-injected with vehicle (saline, blue) or cAMPS-Rp (gray). Two-way RM ANOVA, Ex-4: $F_{(1, 10)}$= 13.1, **p<0.01; cAMPS-Rp: $F_{(1, 10)}$= 8.56, p<0.05; Ex-4 × cAMPS-Rp: $F_{(1, 10)}$= 4.3, p=0.06. **(e)** Mean (± s.e.m.) number of nicotine infusions earned following control microinjection of vehicle (saline) or Ex-4, 2 mm above the IPN (n=6). **(f)** Mean (± s.e.m.) number of nicotine infusions earned following IPN microinjection of vehicle (saline) or Ex-9 (20 μg; n=9). One-way RM ANOVA: $F_{(2, 16)}$=4.3, p<0.05. *P<0.05 compared with vehicle; Bonferroni's test.

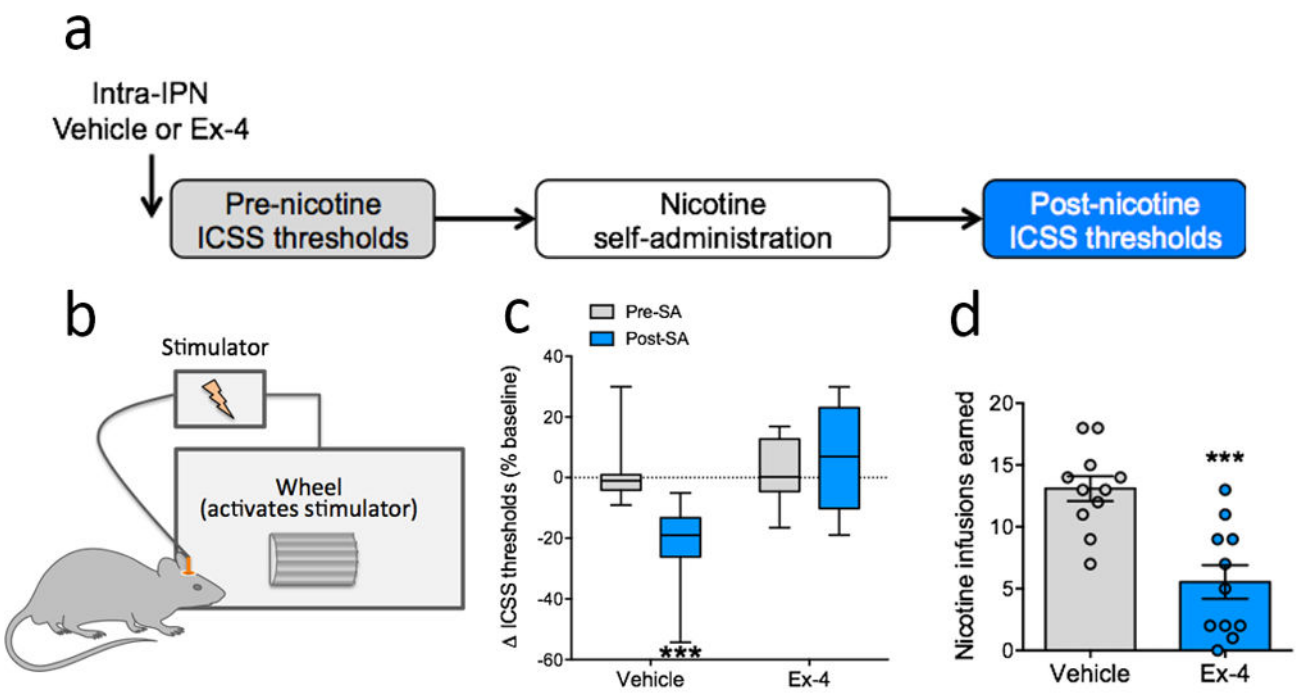

Figure 7. GLP-1 in IPN abolishes nicotine reward

(a) Graphical representation of experimental design. **(b)** Graphical representation of ICSS procedure, in which a rat responds on a wheel manipulandum to receive rewarding intracranial electrical stimulation. The minimally rewarding stimulation intensity that will support reliable responding is termed the reward threshold. **(c)** Mean (± s.e.m.) percentage change from baseline reward thresholds recorded immediately before (gray; pre-nicotine) and after (blue; post-nicotine) nicotine self-administration in animals receiving intra-IPN infusion of vehicle or Ex-4 (0.1 μg/0.5 μl). Two-way RM ANOVA, Nicotine: $F_{(1, 22)}$=5.8, p<0.05; Ex-4: $F_{(1, 22)}$= 11.8, p = 0.01; Nicotine × Ex-4: $F_{(1, 22)}$=11.3, p<0.01. ***P<0.001 compared with pre-nicotine thresholds; Bonferroni's test. **(d)** Mean (± s.e.m.) number of nicotine infusions earned following first ICSS session by rats (n=12) after intra-IPN pretreatment with vehicle (saline) or Ex-4. ***P=0.0002, paired t-test.